Topography and geoid due to lithospheric mass anomalies

Yves Le Stunff[1] and Yanick Ricard[2],*

[1] *Seismographic Station, Department of Geology and Geophysics, University of California, Berkeley, CA 94720, USA*
[2] *Département Terre-Atmosphère-Océan, Ecole Normale Supérieure, 75231 Paris 05, France*

SUMMARY

A model of lithospheric thickness and a recent compilation of Moho depths are used to compute the Earth's isostatic surface topography and associated gravity anomalies. The results are strongly influenced by the uncertainties in lithospheric depth and crustal density profiles. The preferred models explain most of the observed topography and are highly correlated with observed gravity anomalies for harmonic degrees larger than 10. Comparisons of our residual topography with geodynamical calculations of dynamic topography based on mantle circulation are rather poor.

Key words: continental lithosphere, crust, dynamic topography, geoid, isostasy.

INTRODUCTION

It is now widely accepted that the viscous mantle flow associated with thermal convection is responsible for the long-wavelength gravity anomalies observed at the surface of the Earth. In the last two decades, the development of large-scale seismological studies has resolved the broad seismic velocity anomalies in the interior of the Earth. Geophysicists have related them to the observed geoid with quite good agreement and obtained through these calculations some constraints on viscous mantle flow (e.g. Ricard, Fleitout & Froidevaux 1984; Richards & Hager 1984; Forte & Peltier 1987). Nevertheless, the interpretation of the global geoid in terms of mantle mass anomalies was less successful in addressing the following two important questions. Is the surface dynamic topography associated with the flow predicted by dynamic models reasonable? What is the nature of the upper-mantle seismic anomalies?

The surface topography induced by lower-mantle density anomalies has been inferred to be rather similar in pattern to the geoid (e.g. Hager & Clayton 1989) and to have a peak-to-peak amplitude of some 2.5 km. A topography of the same amplitude but closely following the subduction zones around the Pacific has been obtained by Ricard *et al.* (1993). The difference between these two studies comes from the fact that the former infers the mantle density heterogeneities from tomography whereas the latter deduces these heterogeneities from a model of past subductions. The fact that the dynamic topography could be mainly confined to marginal seas and active margins makes it difficult to observe, since these regions can be partly filled with sediments or counterbalanced by hot or wet upper-mantle

wedges in back-arc regions.

Dynamic topography restricted to subduction zones and moving with plate boundaries would agree with two important observations. First, the oceanic floor everywhere follows the same topography versus age relationship, indicating that the long-wavelength topography of deep origin over the ocean basins has a small amplitude. If the flattening of the sea-floor topography at age larger than 100 Ma is associated with lithospheric processes, one should conclude that no dynamic topography is observed (Colin & Fleitout 1990). Even if this flattening is due to deep-mantle effects, only some 500 m peak-to-peak topography can be associated with deep circulation effects (Cazenave & Lago 1991). Second, if large-scale dynamic topography were stationary with respect to plate tectonics, mobile continents would move upward and downward following the dynamic topography undulations. However, geological records indicate that the relative sea-level variations recorded on different platforms should not be larger than about 500 m (Gurnis 1990). This observation is in agreement with models where plates are 'carrying' their dynamic topography.

A recent study (Forte *et al.* 1993) estimated the amplitude of this dynamic topography to be of the order of 6 km peak-to-peak. These authors call dynamic topography the difference between the observed topography and the isostatic crustal topography (i.e. the topography isostatically related to crustal anomalies only). This definition is different from that used in this paper and in the previously quoted papers where the dynamic topography is defined as being that generated by deeper density contrasts outside the upper surface boundary layer of mantle convection. The crucial problem is whether a topography signal in addition to that associated with both crustal and lithospheric anomalies exists or not. This topography should be related to deep-mantle convection and is, in fact, the dynamic topography that various authors have tried to observe

* Now at: Département de Géologie, Ecole Normale Supérieure, 46 allée d'Italie, 69364 Lyon Cedex 07, France.

(Cazenave, Souriau & Dominh 1989; Colin & Fleitout 1990; Gurnis 1990; Cazenave & Lago 1991; Kido & Seno 1994) or predict (e.g. Hager & Clayton 1989; Ricard *et al.* 1993).

Most of the global tomographic models depict seismic velocities under continents as being faster than normal down to depths of 300–400 km (Grand 1987; Su, Woodward & Dziewonski 1992; Zhang & Tanimoto 1993), but it is unclear whether these fast seismic anomalies are associated with dense mantle or not. Part of the continental lithosphere, the tectosphere, may be depleted and chemically lighter than the normal mantle (Jordan 1975). Models trying to fit the global observed geoid assuming that seismic velocity anomalies are directly proportional to mantle density heterogeneities have also reached conflicting conclusions as to the nature of the large-scale heterogeneity of the upper mantle. Whereas Hager & Clayton (1989) and Ricard, Vigny & Froidevaux (1989) have assumed that most of the continental tectosphere is of petrological origin and is not related to very high-density mantle, Forte *et al.* (1993) suggest that these anomalies correspond to very dense material. Following their interpretation, strong downwelling currents are located under cratons, and they explain the gravity low under Laurentides as the result of a surface depression induced by the sinking tectosphere (Peltier *et al.* 1992).

In this study, we estimate an upper bound on dynamic topography and constrain the subcontinental lithospheric density. Using a compilation of crustal thicknesses and a simple model of lithospheric heterogeneities, we compute the associated isostatic topography and geoid and compare them with observations. Our results suggest that dynamic topography related to deep-mantle convection is of low amplitude and that the subcontinental lithosphere is neither very dense nor deep. The geoid signal due to lithospheric mass anomalies has a root mean square amplitude of only 4 m but can locally reach a few tens of metres, in agreement with the results of Hager (1983).

LITHOSPHERIC MASS ANOMALIES

Various sources of lithospheric mass anomalies affect the Earth's topography and geoid. Here, we only consider five sources of shallow density variations. First, the most obvious one is related to the presence of the oceans. Our file of water depth is taken from the ETOPO5 (1992) data base. Second, the huge ice sheets over polar regions, Antartica and Greenland must also be taken into account. Over Antartica, the RAND.SIO (1992) data file of ice thickness is used, and over Greenland, we simply assume that all the topography above sea-level is made of ice. Third, we consider the presence of sediments where data are available. Over oceanic areas, sediment thickness was compiled by Colin (1993). Over Europe and part of Asia, we use a thickness file prepared by Fielding (1993). Fourth, a global data set of crustal thickness has been published by Čadek & Martinec (1991). Their original file includes the sediments in the crustal thickness. For our purpose, we removed our file of sedimentary cover from their crustal thickness. Čadek & Martinec (1991) take results from various seismic studies, and they use a predictor algorithm to fill the gaps between

observations. For the oceanic floor they assumed a crustal thickness increasing with age from 5 km over ridges to 7 km for lithosphere more than 80 Ma old. Following White, McKenzie & O'Nions (1992), we instead choose a constant oceanic thickness of 7 km. However, due to the accumulation of sediments with time, the total crustal thickness increases somewhat with age. Zones of anomalously thick crust, due to hotspot tracks or flood basalts, are corrected for using a compilation by Colin (1993). Over Australia we update the Čadek & Martinec (1991) data file with observations summarized by Dooley & Moss (1988). With all its imperfections, we think that our crustal data file gives a more reliable crustal thickness than that obtained using a simple ocean/continent distribution (Woodhouse & Dziewonski 1984). It is also based on more observations than a previous attempt by Nataf, Nakanishi & Anderson (1986) using observations by Soller, Ray & Brown (1981). The fifth data file needed to complete our set of shallow mass anomalies is the lithospheric thickness. We deduce the lithospheric thickness from the age of the ocean floor and from a regionalization of continent areas. Three types of continental lithosphere are defined following Sclater, Jaupart & Galson (1980): Archean cratons, stable continents and tectonic areas.

We are aware that large uncertainties are present in the crustal thickness data file. The original data are scarce and uneven, and the deepest reflector seen by seismic studies may not be the real Moho. Under continents, however, our knowledge of the crustal thickness is certainly better than our knowledge of lithospheric properties. The depth of the lithosphere is not as well constrained as the crustal depth: the lithosphere–asthenosphere boundary is poorly determined by seismology. Under oceans, several studies show that the thickness of the lithosphere increases with the square root of sea-floor age up to at least 100 Ma (Chapman & Pollack 1977; Parsons & Sclater 1977). Therefore, we chose a simple model in which the lithospheric thickness, e_1, varies with age up to 100 Ma as follows:

$$e_1 = e_{max}\sqrt{age/100}, \qquad (1)$$

where e_{max} is the lithospheric thickness at 100 Ma, and where the age is in Ma. This expression can be deduced from a simple model of half-space cooling. For ages greater than 100 Ma, we assume that the lithospheric thickness remains constant and equal to e_{max}. This constant thickness at old age is intended to simulate what is obtained from a plate cooling model (McKenzie 1967). Such a model is only an approximation to the actual physics where various hotspots might give an excess buoyancy to the old oceanic lithosphere (Carlson & Johnson 1994). However, such a buoyancy associated with hot mantle underplating should also be included among the lithospheric anomalies rather than be associated with the dynamic topography of deep origin. Over continents, we test different density versus depth relationships for each of our continental zones (Archean, stable and tectonic zones). The geographical distribution of the three types of continental zones plus the oceanic zone is depicted in Fig. 1.

Among the five contributions to lithospheric anomalies, the first three are fairly well known or have little effect on the isostatic topography and geoid. Thus, we directly correct
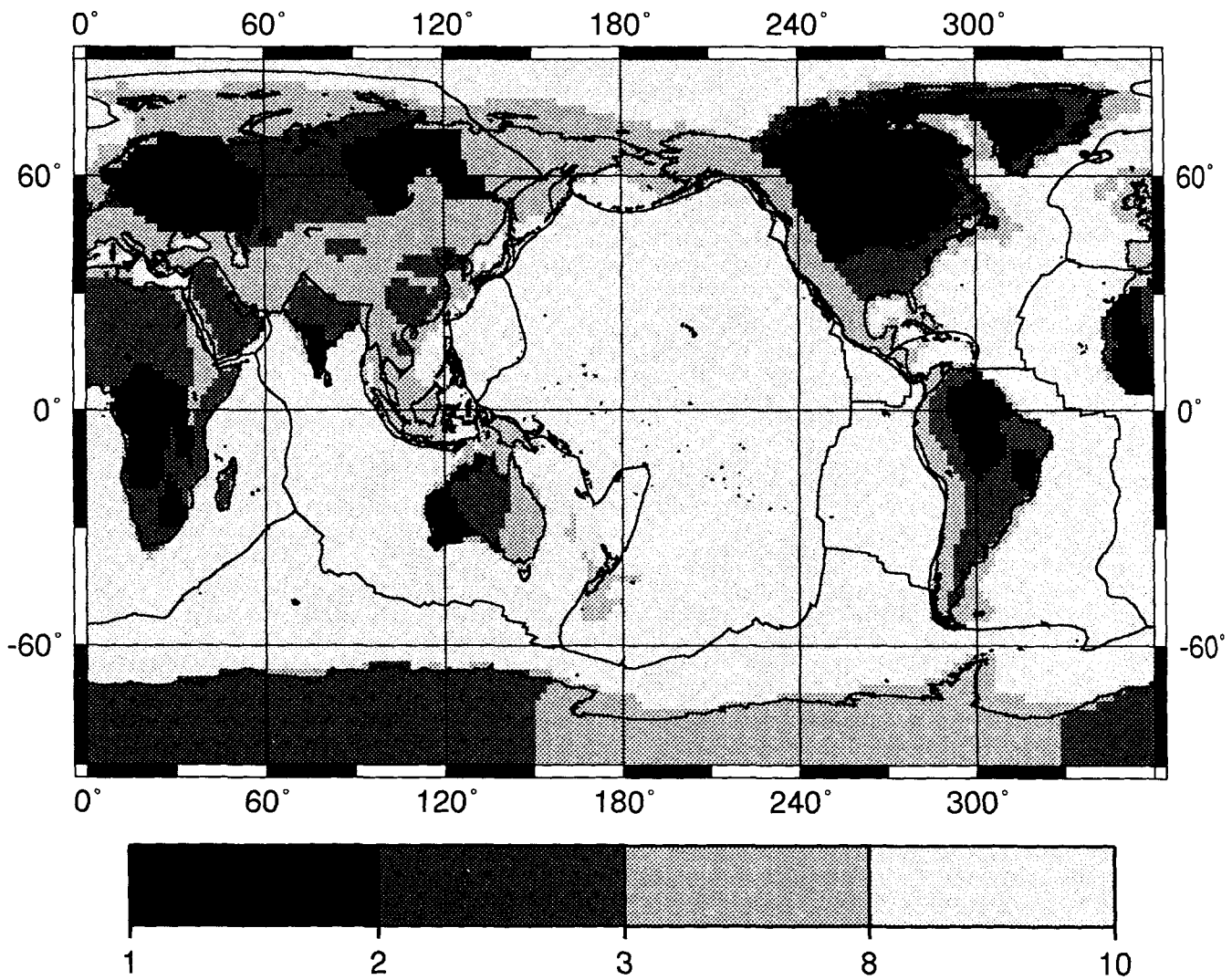
Figure 1. Geographical distribution of the three types of continental zones (1, Archean; 2, stable; 3, tectonic zones) and oceanic zones (8).

the observed topography for the effects of water, ice and sediments. We simply convert these layers of density ρ_i and thickness e_i, into layers of equivalent crust of density ρ_c following the isostatic rule. We call t_0 the observed topography given by the ETOPO5 data set. This topography follows the bottom of the sea, the top of the sediments, the top of the ice sheets. A corrected topography t is computed from t_0 following

$$t = t_0 + e_w \frac{\rho_w}{\rho_c} - e_i \left(1 - \frac{\rho_i}{\rho_c}\right), \tag{2}$$

where e_w and ρ_w are the water depth and density, and where e_i and ρ_i stand for the sediment or ice thickness and density. We chose values of $1000\,\mathrm{kg\,m^{-3}}$, $2500\,\mathrm{kg\,m^{-3}}$ and $1000\,\mathrm{kg\,m^{-3}}$ for the water, sediment and ice densities, respectively. Accordingly, the crustal thickness h_0 is increased to h:

$$h = h_0 + t - t_0. \tag{3}$$

ISOSTATIC TOPOGRAPHY AND GEOID

To compute the topography and the geoid induced by internal mass anomalies, Green functions deduced from a radially stratified viscous earth are often used (Richards & Hager 1984; Ricard *et al.* 1984; Forte & Peltier, 1989). These models are successful in explaining the long-wavelength geoid when a lithospheric viscosity not higher than that of the lower mantle is used. However, the concept of plate tectonics indicates that individual plates behave rigidly. This indicates that the lithosphere is locally much stiffer than what is used in global mantle flow calculations. On a smaller scale the lithosphere is also known to be elastic and to support stresses for millions of years. We do not think that the low or high lithospheric strengths implied by these different approaches are contradictory. On a large scale, the observed plate motion is roughly in phase with the deep-mantle flow, and the existence of lithospheric plates does not impede the flow (Forte & Peltier 1987). On the contrary, for mass anomalies located at shallow depths the lithosphere

may behave like a very highly viscous lid forbidding horizontal surface motions. Of course, only models with plates and laterally variable viscosity will properly reconcile the two aspects. Already, models with independent and rigid plates floating on top of a viscous mantle have shown that mass anomalies beneath plate boundaries induce a gravity signal different from that induced by the same mass anomalies far from plate boundaries. The latter is close to what can be modelled using an elastic lithosphere; the former close to what is obtained by models without lithosphere (Ricard *et al.* 1989).

Therefore, for shallow mass anomalies and for the long wavelengths under consideration, the lithospheric mass anomalies are simply isostatically compensated. In that case, the non-isostatic topography *H* is given by:

$$H = H_0 - \frac{1}{\rho_0} \int_0^D \rho(z) \left(\frac{a - z}{a} \right)^2 dz, \tag{4}$$

where ρ_0 is the upper-crust density and *a* the earth radius. The integral is performed from the surface of the earth to a depth *D* equal to the maximum depth of location of lithospheric mass anomalies. H_0 is a reference value such that the average of the non-isostatic topography *H* over the sphere is zero. In the case of a perfectly compensated topography, the integral in eq. (4) is everywhere constant and equal to H_0, and the non-isostatic topography is zero.

The geoid undulation due to an isostatically compensated mass distribution is simply related to the products of the density anomalies times their compensation depths (Turcotte & Schubert 1982). For a spherical self-gravitating earth, Hager (1983) has shown that the geoid height coefficients N_{lm} of degree *l* and order *m* are closely approximated by

$$N_{lm} = \frac{-2\pi G}{g} \frac{(l + 0.6)}{(l + 0.5)} \int_0^D \delta\rho_{lm}(z) \left(z - \frac{l + 3}{2} \frac{z^2}{a} \right) dz, \tag{5}$$

where $\rho_{lm}(z)$ is the depth-dependent coefficient of the expansion of the density in spherical harmonics, *G* the gravitational constant and *g* the average surface gravity.

LEAST-SQUARES INVERSION

Using eqs (4) and (5), we can try to invert for the density anomalies $\delta\rho_{lm}(z)$ by fitting both the observed geoid and topography. The fit of these two quantities should, in principle, give us both the average density and thickness of the lithosphere since the sensitivities with depth of the two observables are different. In what follows, we assume that our lithospheric density is determined by the knowledge of a finite set of parameters: the upper continental crust density (from the surface to two-fifths of the total crust thickness), the middle continental crust density (from two-fifths to four-fifths of the total crust thickness), the lower continental crust density (the last fifth of the total crust thickness), the oceanic crustal density, the thickness of the oceanic lithosphere of age greater than 100 Ma (parameter e_{max} of eq. 1), the density of oceanic lithosphere, and the thickness and density of the cratons. The density and the thickness of active continental lithosphere are assumed to be the same as those of the old oceans. The parameters defining the stable

continental region are the same either as those of the cratons or as those of the old oceans.

The geoid is dominated by the signature of deep-mantle anomalies (e.g. Hager & Clayton 1989) and/or subducted slabs (e.g. Ricard *et al.* 1993), not by the lithospheric heterogeneities. We should therefore only try to fit the geoid at degrees larger than say 10, where the correlation between geoid and topography starts to be significant. The strong decrease of the geoid spectrum with increasing degree compels us to use the free air gravity instead of the geoid. The free air gravity, the spectral coefficients of which are obtained by multiplying those of the geoid by $g(l - 1)/a$, has a much flatter spectrum. We have verified that fitting the free air gravity for degrees larger than l_{min} gives the same results for l_{min} between 10 and 20. Therefore, we invert for the various parameters by minimizing the non-isostatic topography between degrees 1 and 24, and fitting the free air gravity between degrees 13 and 24.

The best-fitting parameters are obtained by minimization of the following quantity:

$$I(\mathbf{p}) = [\mathbf{d}_0 - g(\mathbf{p})]^t \mathbf{C}_{d_0 d_0}^{-1} [\mathbf{d}_0 - g(\mathbf{p})]$$
$$+ (\mathbf{p} - \mathbf{p}_0)^T \mathbf{C}_{p_0 p_0}^{-1} (\mathbf{p} - \mathbf{p}_0), \tag{6}$$

where **p** is the vector of the unknowns, $\mathbf{d}_0$ is the data field vector including an expansion of the topography and the free air gravity, and $g(\mathbf{p})$ represents the corresponding synthetic fields. The exponent *T* refers to the transposed vector or matrix. Our *a priori* knowledge of the parameters enters both in an *a prior* solution $\mathbf{p}_0$ and a covariance $\mathbf{C}_{p_0 p_0}$. On its diagonal, this matrix contains the squares of the uncertainties $\Delta\mathbf{p}$, i.e. the variance of the model parameters. The matrix $\mathbf{C}_{d_0 d_0}$ ensures the correct dimensionalization of the equation. Eq. (6) is solved by an iterative procedure (Tarantola & Valette 1982).

RESULTS

We start from the following *a priori* parameter vector: upper continental crust density $2720 \pm 60 \, \text{kg m}^{-3}$, middle continental crust density $2920 \pm 130 \, \text{kg m}^{-3}$, and lower continental crust density $3020 \pm 140 \, \text{kg m}^{-3}$. These crustal values are taken from Holbrook, Mooney & Christensen (1992). For the oceanic crustal density, we take $2920 \pm 40 \, \text{kg m}^{-3}$. The *a priori* oceanic lithosphere is characterized by a maximum thickness of $100 \pm 10 \, \text{km}$ and a density of $3380 \pm 20 \, \text{kg m}^{-3}$. The density of the asthenosphere is $3300 \, \text{kg m}^{-3}$. Regarding the properties of the continental lithosphere we make four different assumptions. First, the stable and tectonic continental areas have the same properties (density and depth) as the old oceanic lithosphere, whereas the continental lithosphere under cratons is $250 \pm 100 \, \text{km}$ thick and has a density of $3360 \, \text{kg m}^{-3}$ (model 1). The second case is identical to the first one except that the continental lithosphere now has a density decreasing linearly between $3380 \, \text{kg m}^{-3}$ at the surface and the asthenospheric density of $3300 \, \text{kg m}^{-3}$ at 250 km depth (model 2). Third, tectonic continental areas and old oceans have the same properties, stable continents and cratons are 250 km thick with a uniform density of $3360 \, \text{kg m}^{-3}$ (model 3). For the fourth case, the density varies linearly with depth under stable continents and

cratons between $3380 \, \text{kg m}^{-3}$ at the surface and $3300 \, \text{kg m}^{-3}$ at 250 km depth (model 4).

The different *a priori* (in parentheses) and inverted density profiles are summarized in Table 1. The four columns correspond to the four assumptions. The last two lines give the variance reduction achieved by the model for the topography (between degrees 1 and 24) and for the free air gravity (between degrees 13 and 24). All models clearly give a very good fit to the topography but only explain a small fraction of the free air gravity signal. All models predict an oceanic lithospheric thickness less than 100.3 km, a value that agrees with the analysis of heat flow and detailed sea-floor topography (Stein & Stein 1992). The values for the continental lithospheric thickness are always much smaller than what is often claimed by seismologists, and the continental lithospheric densities are less (less on average for models 4 and 2) than those for the old oceanic lithosphere.

The uncertainties chosen for the inversion, in particular for the crustal density values, roughly correspond to what is observed by petrologists (Holbrook *et al.* 1992). An increase of all the uncertainties by a factor of 2 does not significantly affect either the *a posteriori* values of the parameters (by less than 1 per cent) or the fit to observations (a 1 per cent better topography, a 2 per cent better geoid). The choice of much larger *a priori* variances (e.g. five times larger) leads to numerical instabilities showing the strong trade-offs between parameters, for example between the densities of the oceanic crust and of the oceanic lithosphere.

In Table 2, we compute the average non-isostatic topography and a rough value of the geoid obtained on top of different tectonic regions (oceanic areas younger than 20 Ma, oceanic areas between 100 and 140 Ma, cratons, stable continents and tectonic zones). These non-isostatic topographies have been computed from eq. (4) and assuming the stable continent region as the zero reference level. For the geoid, an estimate has been obtained assuming that the *l*-dependent fraction in front of the integral is equal to 1 and that there is no *l*-dependence in the integral. We use the results of model 4, which is the model reaching the best variance reduction, for both topography and geoid. We predict for each area a non-isostatic topography equal within

Table 2. Computed non-isostatic topography in metres (stable continents are 0-level) and isostatic geoid in metres (young oceans are 0-level). Results of Model 4 are used.

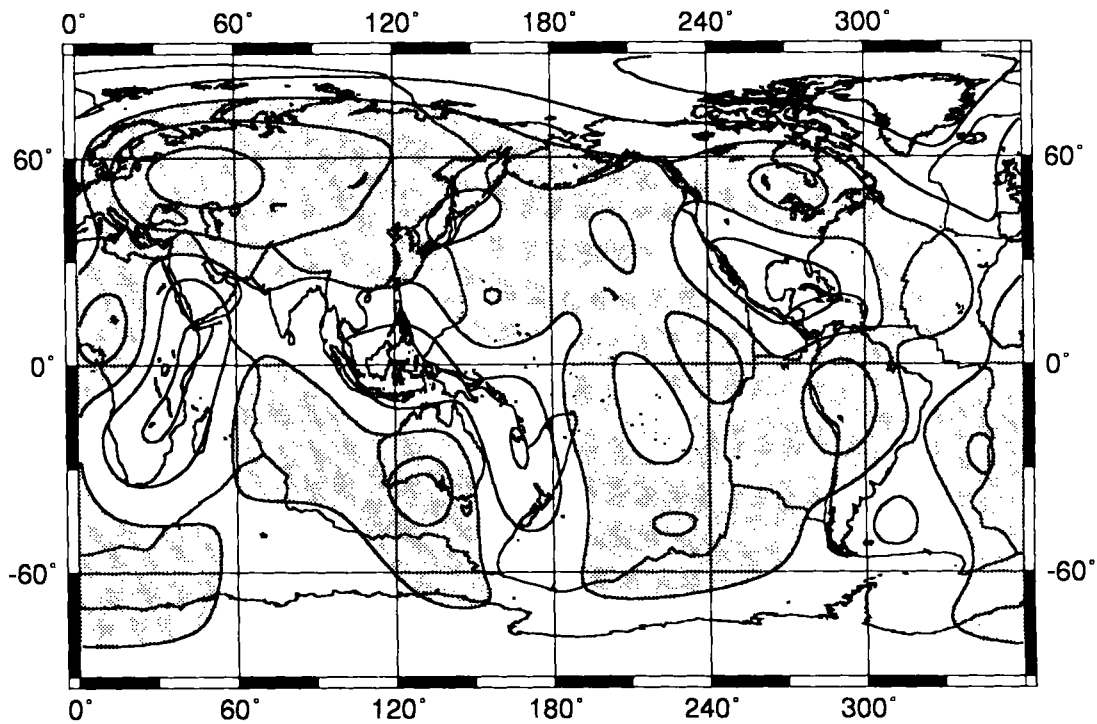|	Non-Isostatic Topography	Isostatic Geoid
Young Oceans	231 m	0 m
Old Oceans	552 m	-8.9 m
Cratons	-272 m	-8.3 m
Stable Continents	0 m	-9.5 m
Tectonic Zones	169 m	-1.5 m

a few hundred metres to that of the reference level. For the geoid, undulations of rather small amplitude are predicted in agreement with a previous study (Hager 1983). The geoid decreases by around 10 m between young and old oceans (Turcotte & Schubert 1982), and the geoid low over cratons is comparable to that over old oceans. The difference of geoid heights over cratons and ridges could be even smaller if the geoid lows over the Canadian and Scandinavian cratons are due to postglacial depressions. The existence of a geoid low over cratons of only a few metres would imply that the tectosphere density is very low, in agreement with the findings of Doin, Fleitout & Colin (1992).

Inspection of the values of Table 2 shows that the integrated lithospheric density over a cratonic column closely matches that over an old ocean column. This indicates that the crust, by itself, is isostatically compensated in our models. The lateral density variations in the mantle lithosphere are only responsible for the ridge topography. This result is in complete disagreement with Forte *et al.* (1993), who suggest that without the presence of a thick dense lithosphere, cratons would be some 2 km above their present height. The discrepancy arises from the higher density in the continental crust in our models. The choice of an average crustal density of $2900 \, \text{kg m}^{-3}$ instead of $2800 \, \text{kg m}^{-3}$ for cratons having a typical crustal thickness of

Table 1. Results of different inversions in terms of parameters (densities are in kg m^{-3} and depths in km), topography variance reduction (degrees 1–24) and geoid variance reduction (degrees 13–24). The *a priori* parameters and variance reductions are in parentheses. Dashes stand for negative geoid variance reductions. Model 1: craton (constant); Model 2: craton (linear); model 3: craton + stable (constant); model 4: craton + stable (linear). For Models 2 and 4, the continental lithosphere density varies linearly with depth and the values written in the table correspond to the lithospheric density extrapolated at the surface.

	Model 1	Model 2	Model 3	Model 4
$\rho_{\text{upper.crust}}$	$2723_{(2720)}$	$2723_{(2720)}$	$2742_{(2720)}$	$2722_{(2720)}$
$\rho_{\text{middle.crust}}$	$2953_{(2920)}$	$2954_{(2920)}$	$2946_{(2920)}$	$2946_{(2920)}$
$\rho_{\text{lower.crust}}$	$3052_{(3020)}$	$3053_{(3020)}$	$3044_{(3020)}$	$3045_{(3020)}$
$\rho_{\text{aver.crust}}$	$2880_{(2860)}$	$2881_{(2860)}$	$2884_{(2860)}$	$2876_{(2860)}$
$\rho_{\text{ocean.crust}}$	$2922_{(2920)}$	$2923_{(2920)}$	$2920_{(2920)}$	$2920_{(2920)}$
$\rho_{\text{ocean.litho}}$	$3359_{(3380)}$	$3358_{(3380)}$	$3360_{(3380)}$	$3359_{(3380)}$
$\text{Depth}_{\text{ocean.litho}}$	$100.3_{(100)}$	$99.22_{(100)}$	$97.5_{(100)}$	$96.33_{(100)}$
$\rho_{\text{cont.litho}}$	$3337_{(3360)}$	$3369_{(3380)}$	$3337_{(3360)}$	$3368_{(3380)}$
$\text{Depth}_{\text{cont.litho}}$	$165.3_{(250)}$	$221.8_{(250)}$	$168.4_{(250)}$	$217.0_{(250)}$
Topography VR	$84.8\%_{(73.8\%)}$	$84.8\%_{(81.9\%)}$	$85.7\%_{(62.8\%)}$	$85.5\%_{(82.9\%)}$
Geoid VR	$14.7\%_{(-)}$	$17\%_{(-)}$	$20.3\%_{(-)}$	$21.9\%_{(13\%)}$

(a) NON ISOSTATIC TOPOGRAPHY (Degrees 1-8)
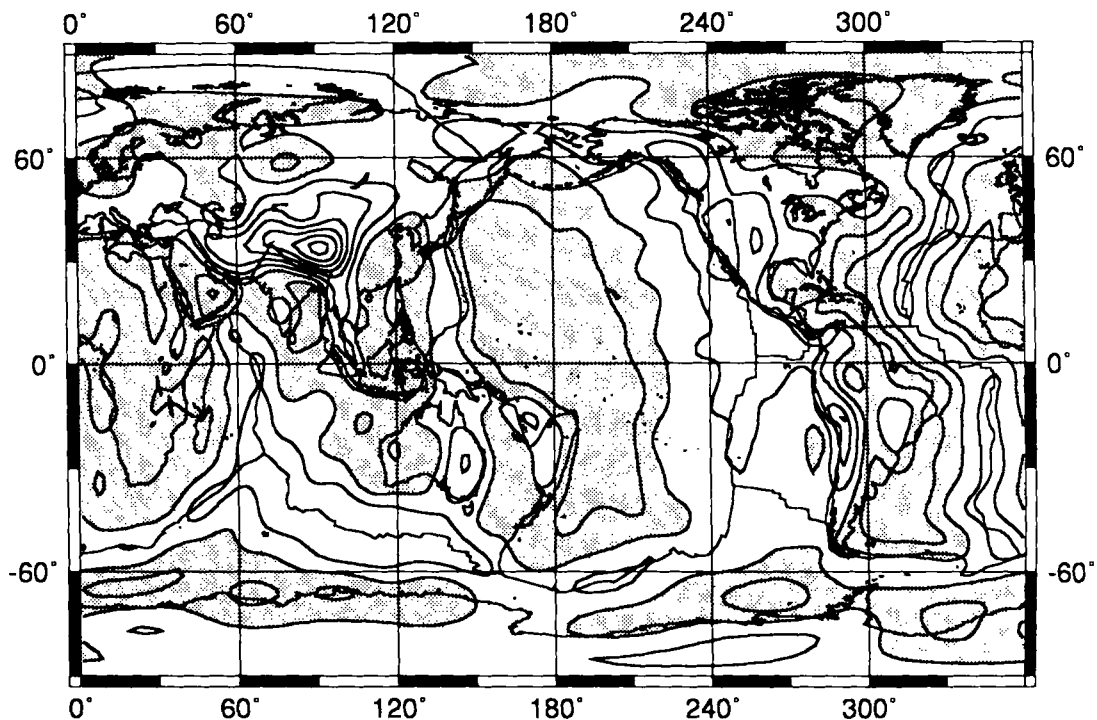

(b) ISOSTATIC GEOID (Degrees 2-24)

Figure 2. (a) Non-isostatic topography (observed minus inverted isostatic topography using model 4) between degrees 1 and 8. The level lines are 500 m apart. The topographic highs are white, the topographic lows are shaded with a light grey. The maximum value is +1280 m; the minimum value is −1210 m. (b) Synthetic isostatic geoid between degrees 2 and 24. The level lines are 4 m apart. The isostatic geoid is maximum over topographic highs like the ridges or the Tibetan plateau. The maximum value is +25.6 m; minimum value is −8.7 m.
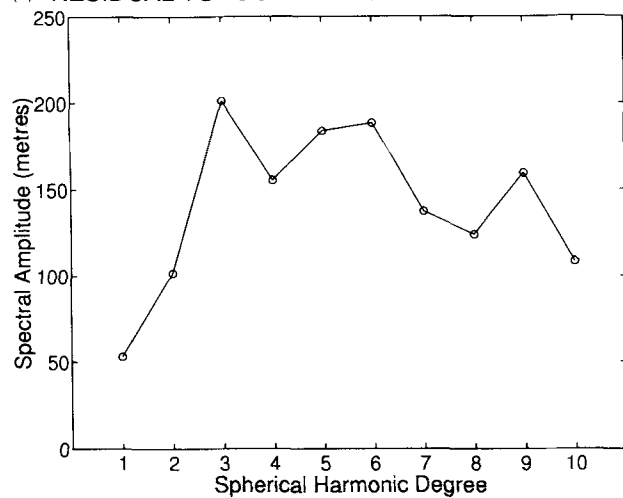
40 km, leads to some 1.5 km of topography difference. In other words, the difference is a matter of a currently observationally unresolvable difference in the choice of a lower-crust density.

Figure 2(a) depicts the non-isostatic topography (between degrees 2 and 8) predicted by model 4. This topography has a peak-to-peak amplitude of 2400 m but a low root mean square amplitude of 425.75 m. This topography is dominated by medium-wavelength features. Some of them have clear geophysical meanings, like the African high plateaus. However, this residual topography does not clearly correlate with any of the dynamic topographies that have been inferred from circulation models of the mantle. The geoid obtained from the lithospheric density model 4 is depicted in Fig. 2(b). Its amplitudes over the different tectonic provinces correspond to those described in Table 2. It clearly demonstrates, once more, the rather negligible amplitude of the geoid signal arising from the near-surface anomalies. Its root mean square amplitude, being only 3.97 m, is to be compared to the root mean square amplitude of the observed geoid of 41.71 m.

The spectral amplitude of the residual topography of Fig. 2(a) is shown in Fig. 3(a) for the first 10 degrees. The amplitudes, which are less than 200 m, should be indicative of those of the dynamic topography that might be induced by deep-mantle circulation. It is worth noticing that, whereas the observed geoid is largest at degree 2 and is commonly attributed to deep-mantle sources, the non-isostatic topography for the same degree is particularly low. The correlation between the geoid due to lithospheric sources (Fig. 2b) and the observed geoid is depicted in Fig. 3(b). This correlation exceeds the 95 per cent confidence level (dashed line) for all degrees larger than 9 (except for degree 12). It is precisely for degrees smaller than 9 that a satisfactory model of the geoid can be obtained from deep mantle origin (e.g. Ricard *et al.* 1993).

DISCUSSION

The existence of long-wavelength topography related to the deep-mantle circulation is still a puzzling problem after some 10 years of investigation. Over oceans, various studies (e.g. Colin & Fleitout 1990; Stein & Stein 1992; Kido & Seno 1994) have confirmed that, if it exists, a topographic signal different from that of normal sea-floor cooling is weak (less than 500 m). Under old continents the evidence of downgoing flow associated with a dense and thick lithosphere suggested by Forte *et al.* (1993) is dependent upon their assumption of a rather light lower crust. With a somewhat denser but equally reasonable crustal density value, we suggest on the contrary that the subcratonic lithosphere is neither very dense nor very thick. A dense and deep tectosphere would induce geoid lows which are not observed in the wavelength band where the geoid correlates with surface features ($l > 10$). Forte *et al.* (1992) do not obtain these excessive gravity lows only because they use compensation models in which the lithosphere is very weak. We think this is inappropriate for modelling the effect of near-surface density heterogeneities that are tightly embedded in the lithosphere.

To quantify the trade-off between the crustal density and the properties of the continental lithosphere we kept constant the values of the oceanic parameters (crustal density, lithospheric thickness and density), chose various continental densities and only inverted for the properties of the continental lithosphere (keeping the assumptions of model 4). The results are depicted in Fig. 4. On top are the variance reductions for the topography and the geoid. The two curves have a maximum for an average crustal density of about 2900 kg m^{-3}. The bottom panel shows the density and thickness of the lithosphere below cratons as a function of the assumed continental crustal density: these two parameters decrease as the continental crust becomes denser. This shows that there is a simple trade-off between crustal density and continental lithospheric thickness.

In this paper we have tried to minimize the topography not related to lithospheric density. This may not be the best way to proceed if indeed the dynamic topography due to

(a) **RESIDUAL TOPOGRAPHY SPECTRAL AMPLITUDE**
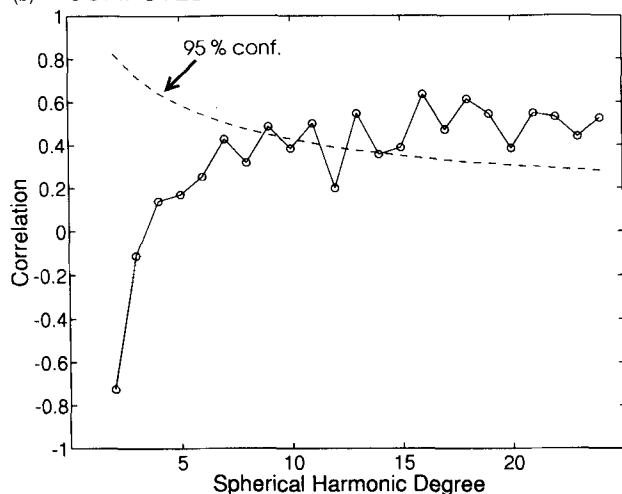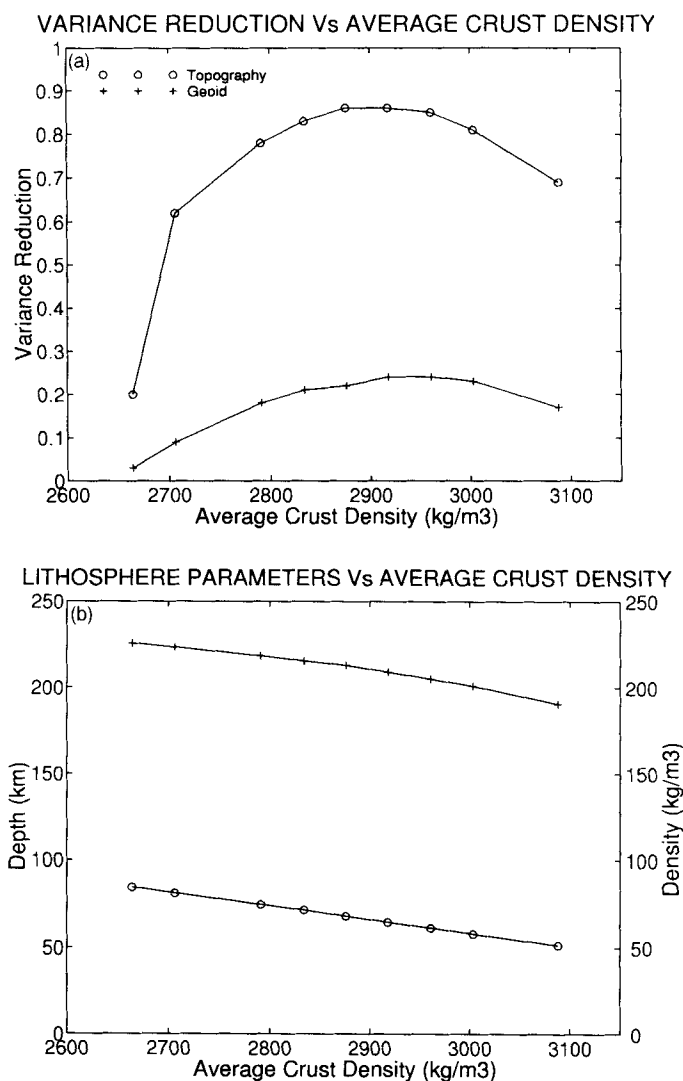
(b) **COMPUTED/OBSERVED GEOID CORRELATION**

Figure 3. (a) Spectral amplitude of the non-isostatic topography. The low amplitudes indicate that the dynamic topography related to deep mantle circulation should be very small. (b) Correlation coefficients between synthetic and observed geoids for degrees 2–24. The dashed line is the 95 per cent confidence level. For degrees larger than 10 most of the geoid signal is simply related to isostatically compensated lithospheric mass anomalies.

VARIANCE REDUCTION Vs AVERAGE CRUST DENSITY

LITHOSPHERE PARAMETERS Vs AVERAGE CRUST DENSITY

Figure 4. (a) Variance reduction for topography (circle) and geoid (plus) as a function of the average continental crustal density. (b) Best density excess (circle) (relative to the $3300\,\mathrm{kg\,m^{-3}}$ of the asthenosphere) in $\mathrm{kg\,m^{-3}}$ and thickness (plus) in kilometres of lithosphere under cratons and stable continents (model 4) as a function of the average continental crustal density.

deep mass anomalies correlates with one of our tectonic provinces. As none of these provinces obviously correlates with either the geoid or the lower-mantle heterogeneity pattern deduced from tomography, our results suggest that none of the dynamic models predicting a dynamic topography rather similar to the geoid pattern (e.g. Hager & Clayton 1989) is acceptable. The possibility of a dynamic topography only related to subduction zones (Ricard *et al.* 1993) is more difficult to rule out since the dynamic topography possible associated with back-arc basins is difficult to estimate. However, we clearly do not see any general topographic depression following the subduction zones in our residual topography.

We tried various inversions with other parametrizations: we added independent parameters for the tectonic continental areas, we divided this domain into compressional and extensional domains, we assumed that the thickness of the oceanic lithosphere follows a square root of age law at all ages, etc. The conclusions are not significantly different: the lower crust is rather dense, the continental

lithosphere is thinner than 250 km and lighter than the oceanic lithosphere, the geoid heights over old oceans and cratons are similar and the non-isostatic topography has a small amplitude. The patterns found for the non-isostatic topography are similar to that of Fig. 2(a) and do not support any of the previously proposed models of long-wavelength dynamic topography related to deep-mantle circulation.

ACKNOWLEDGMENTS

REFERENCES

Čadek, O. & Martinec, Z., 1991. Spherical harmonic expansion of the Earth's crustal thickness up to degree and order 30, *Stud. Geophys. et Geod.*, **35**, 151–165.

Carlson, R.L. & Johnson, H.P., 1994. On modelling the thermal evolution of the oceanic upper mantle: an assessment of the cooling plate model, *J. geophys. Res.*, **99**, 3201–3214.

Cazenave, A. & Lago, B., 1991. Long wavelength topography, seafloor subsidence and flattening, *Geophys. Res. Lett.*, **18**, 1257–1260.

Cazenave, A., Souriau, A. & Dominh, K., 1989. Global coupling of Earth surface topography with hotspots, geoid and mantle heterogeneitics, *Nature*, **340**, 54–57.

Chapman, D.S. & Pollack, H.N., 1977. Regional geotherms and lithospheric thickness, *Geology*, **5**, 265–268.

Colin, P., 1993. Géoide global, topographie associée et structure de la convection dans le manteau terrestre: modèlisation et observations, *PhD thesis*, Université Paris 7.

Colin, P. & Fleitout, L., 1990. Topography of the ocean floor: thermal evolution of the lithosphere and interaction of mantle heterogeneities with the lithosphere, *Geophys. Res. Lett.*, **11**, 1961–1964.

Doin, M.-P., Fleitout, L. & Colin, P., 1992. Thermal and petrological structure of old cratons from a study of geoid anomalies, *Ann. Geophys.*, Abstract, **10**, 85.

Dooley, J.C. & Moss, F.J., 1988. Deep crustal reflections in Australia 1957–1973; II, Crustal models, *Geophys. J.*, **93**, 239–249.

ETOPO5, 1992. Bathymetry/Topography Data. NOAA-NGDC, Data Announcement 88-MGG-02, US Department of Commerce.

Fielding, 1993. *Cornell Server for ARPA-related File.*

Forte, A.M. & Peltier, W.R., 1987. Plate tectonics and aspherical earth structure: The importance of poloidal–toroidal coupling, *J. geophys. Res.*, **92**, 3645–3679.

Forte, A.M., Woodward, R.L., Dziewonski, A.M. & Peltier, W.R., 1992. 3-D models of mantle heterogeneity derived from joint inversions of seismic and geodynamic data, *EOS, Trans. Am. geophys. Un.*, **73**, Spring Meeting suppl., 200.

Forte, A.M., Peltier, W.R., Dziewonski, A.M. & Woodward, R.L., 1993. Dynamic topography: a new interpretation based upon mantle flow models derived from seismic tomography, *Geophys. Res. Lett.*, **20**, 225–228.

Grand, S.P., 1987. Tomographic inversion for shear velocity beneath the North American plate, *J. geophys. Res.*, 14 065–14 090.

Gurnis, M., 1990. Bounds on global dynamic topography from Phanerozoic flooding of continental platforms, *Nature*, **344**, 754–756.

Hager, B.H., 1983. Global isostatic geoid anomalies for plate and boundary layer models of the lithosphere, *Earth planet. Sci. Lett.*, **63**, 97–109.

Hager, B.H., & Clayton, R.W., 1989. Constraints on the structure of mantle convection using seismic observations, flow models and the geoid, in *Mantle Convection: Plate Tectonics and Global Dynamics*, pp. 657–763, ed. Peltier, W.R., Gordon and Breach, New York.

Holbrook, W.S., Mooney, W.D. & Christensen, N.I., 1992. The seismic velocity structure of the deep continental crust, in *Continental Lower Crust*, pp. 1–43, eds Fountain, Arculus & Kay, Elsevier.

Jordan, T.H., 1975. The continental tectosphere, *Rev. Geophys. Space Phys.*, **13**, 1–12.

Kido, M. & Seno, T., 1994. Dynamic topography compared with residual depth anomalies in oceans and implications for age–depth curves, *Geophys. Res. Lett.*, **21**, 717–720.

McKenzie, D.P., 1967. Some remarks on heat flow and gravity anomalies, *J. geophys. Res.*, **72**, 6261–6273.

Nataf, H.-C., Nakanishi, I. & Anderson, D.L., 1986. Measurements of mantle wave velocities and inversion for lateral heterogeneities and anisotropy. 3. Inversion, *J. geophys. Res.*, **91**, 7261–7307.

Parsons, B. & Sclater, J.G., 1977. An analysis of the variation of ocean floor bathymetry and heat flow with age, *J. geophys. Res.*, **82**, 803–827.

Peltier, W.R., Forte, A.M., Mitrovica, J.X. & Dziewonski, A.M., 1992. Earth's gravitational field: seismic tomography resolves the enigma of the Laurentian anomaly, *Geophys. Res. Lett.*, **19**, 1555–1558.

RAND.SIO, 1992. *NOAA-NGDC, GEODAS Marine Geophysical Data*, CD-ROM.

Ricard, Y., Fleitout, L. & Froidevaux, C., 1984. Geoid heights and lithospheric stresses for a dynamic Earth, *Ann. Geophys.*, **2**, 267–286.

Ricard, Y., Vigny, C. & Froidevaux, C., 1989. Mantle heterogeneities, geoid, and plate motion: a Monte Carlo inversion, *J. geophys. Res.*, **94**, 17 543–17.559.

Ricard, Y., Richards, M.A., Lithgow-Bertelloni, C. & Le Stunff, Y., 1993. A geodynamic model of mantle density heterogeneity, *J. geophys. Res.*, **98**, 21 895–21 909.

Richards, M.A. & Hager, B.H., 1984. Geoid anomaly in a dynamic Earth, *J. geophys. Res.*, **89**, 5987–6002.

Sclater, J.G., Jaupart, C. & Galson, D., 1980. The heat flow through oceanic and continental crust and the heat loss of the Earth, *Rev. Geophys.*, **18**, 269–311.

Soller, D.R., Ray, R.D. & Brown, R.D., 1981. A global crustal thickness map, *EOS, Trans. Am. geophys. Un.*, **62**, Spring Meeting suppl., 328.

Stein, C.A. & Stein, A., 1992. A model for the global variation in oceanic depth and heat flow with lithospheric age, *Nature*, **359**, 123–129.

Su, W.-J., Woodward, R.L. & Dziewonski, A.M., 1992. Joint inversions of travel-time and waveform data for the 3-D models of the Earth up to degree 12. *EOS, Trans. Am. geophys. Un.*, **73**, Spring Meeting suppl., 201.

Tarentola, A. & Valette, B., 1982. Generalized non linear inverse problems solved using the least squares criterion, *Rev. Geophys.*, **20**, 219–232.

Turcotte, D.L. & Schubert, G. (eds), 1982. *Geodynamics. Applications of Continuum Physics to Geological Problems*, Wiley, New York.

White, R.S., McKenzie, D.P. & O'Nions, R.K., 1992. Oceanic crustal thickness from seismic measurements and rare earth element inversions, *J. geophys. Res.*, **97**, 19 683–19 715.

Woodhouse, J.H. & Dziewonski, A.M., 1984. Mapping the upper mantle: three dimensional modeling of Earth structure by inversion of seismic waveforms, *J. geophys. Res.*, **89**, 5953–5986.

Zhang, Y.S. & Tanimoto, T., 1993. High-resolution global upper mantle structure and plate tectonics, *J. geophys. Res.*, **98**, 9783–9823.